Journal of Magnetic Resonance 211 (2011) 221–227

Contents lists available at ScienceDirect

Journal of Magnetic Resonance

journal homepage: www.elsevier.com/locate/jmr

Use of polyphase continuous excitation based on the Frank sequence in EPR

Mark Tseitlin [a], Richard W. Quine [b], Sandra S. Eaton [a], Gareth R. Eaton [a,*]

[a] Department of Chemistry and Biochemistry, University of Denver, Denver, CO 80208, United States
[b] School of Engineering and Computer Science, University of Denver, Denver, CO 80208, United States

ARTICLE INFO

Article history:
Received 8 March 2011
Revised 14 May 2011
Available online 12 June 2011

Keywords:
EPR
Frank sequence
Polyphase continuous excitation

ABSTRACT

Polyphase continuous excitation based on the Frank sequence is suggested as an alternative to single pulse excitation in EPR. The method allows reduction of the source power, while preserving the excitation bandwidth of a single pulse. For practical EPR implementation the use of a cross-loop resonator is essential to provide isolation between the spin system and the resonator responses to the excitation. Provided that a line broadening of about 5% is acceptable, the cumulative turning angle of the magnetization vector generated by the excitation sequence can be quite large and can produce signal amplitudes that are comparable to that achieved with a higher power 90° pulse.

1. Introduction

In typical pulse NMR and EPR experiments the spins are excited with short high-power pulses. High-power amplifiers are expensive and for in vivo applications it is desirable to decrease power deposition to meet restrictions on the specific absorption rate. One approach that has been demonstrated to decrease power requirements is stochastic excitation [1–4]. It has also been shown that substitution of a short 90° pulse by a series of lower intensity pulses with phases selected with the Frank sequence allowed substantial reduction in peak excitation power in NMR spectroscopy, while maintaining the same excitation bandwidth [5].

In a magnetic resonance experiment with a single on-resonance pulse of length t_p, the rf (microwave) magnetic field B_1 turns the net magnetization vector by an angle:

$$\alpha = \gamma B_1 t_p, \tag{1}$$

where γ is the electron or nuclear gyromagnetic ratio and α is in radians. The power required to achieve turning angle α is given by:

$$\text{power} = D\alpha^2/t_p^2, \tag{2}$$

where D is a parameter that can be measured for a resonator/sample combination with a particular coupling [6]. This expression shows that the power requirement is proportional to α^2, which makes the small turning angles of the Frank sequence advantageous. Typical electron spin relaxation times are orders of magnitude shorter than proton NMR relaxation times, which requires that pulsed EPR experiments are performed with t_p orders of magnitude shorter than for NMR. Since power increases inversely proportional to t_p^2, the peak power required for EPR experiments is substantially greater than for NMR, and reducing the required power is even more advantageous than in NMR. Depending on the efficiency of the resonator, the coupling of the resonator and the lengths of the pulses, the peak power for pulse EPR experiments may be in the kilowatts.

To explore whether the Frank sequence of polyphase excitation could be used in EPR, an experiment was conducted with 256 small turning-angle pulses for an aqueous sample of a triarylmethyl radical [7]. The present paper reports calculations that were performed to examine the following aspects of polyphase excitation and detection: (i) optimization of excitation power; (ii) comparison of (a) data analysis by cross-correlation with the Fourier transform of the excitation phase sequence and (b) deconvolution with the Fourier transform of the excitation waveform including the pulse profile; (iii) spectral distortion due to deviation of the spin response from linearity; and (iv) comparison with single-pulse excitation. Experiments were done at 250 MHz for triarylmethyl radicals and at 1 GHz for lithium phthalocyanine (LiPc) to test the predictions concerning power and deviation from linearity. A block diagram for the experiments and data analysis is shown in Fig. 1. Details are provided in the following paragraphs.

2. Samples and spectroscopy

At 250 MHz the samples were 0.2 mM aqueous solutions of the trityl radical OX63 (methyl tris(8-carboxy-2,2,6,6-tetra(hydroxyethyl)-benzo[1,2-d:4,5-d′]bis(1,3)-dithiol-4-yl)-tripotassium salt) [8] in a 16 mm o.d. tube or the deuterated analog OX63-d_{24} in a 25 mm o.d. tube. Both samples were purged with N_2 and flame-sealed. Lithium phthalocyanine (LiPc) prepared electrochemically

* Corresponding author. Address: Department of Chemistry and Biochemistry, University of Denver, 2101 E. Wesley Ave., Denver, CO 80208, United States. Fax: +1 303 871 2254.
E-mail address: geaton@du.edu (G.R. Eaton).

1090-7807/$ - see front matter © 2011 Elsevier Inc. All rights reserved.
doi:10.1016/j.jmr.2011.06.005

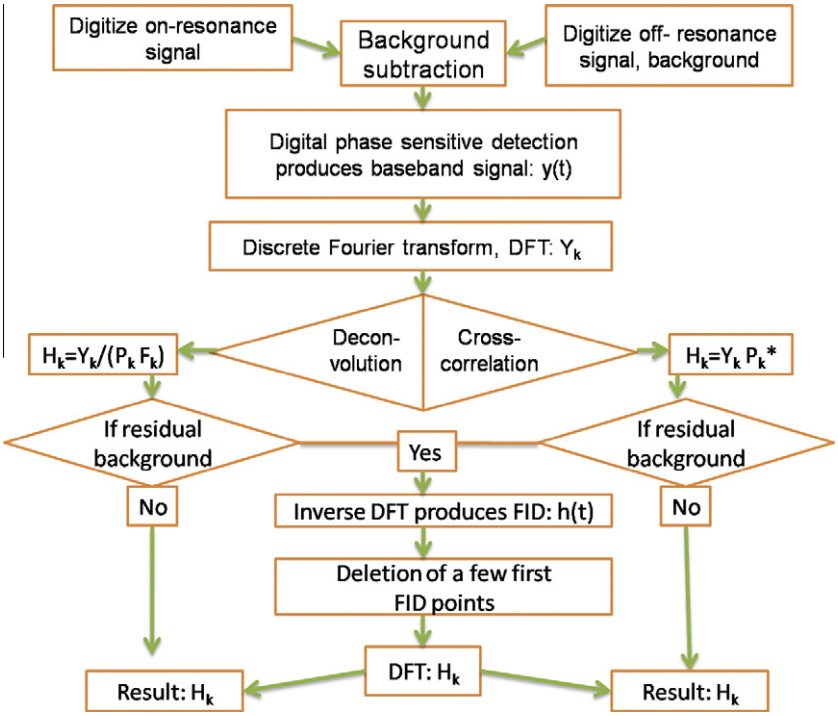

Fig. 1. Block diagram of the polyphase continuous excitation data acquisition and analysis.

following procedures in the literature [9,10] was provided by Prof. Swartz, Dartmouth University. For the 1 GHz experiments multiple small crystals of LiPc were placed in a 3 mm o.d. tube. The tube was extensively evacuated and then flame sealed.

CW experiments at 250 MHz were performed with a reflection resonator that has been described previously [11]. To provide isolation between the spin excitation and detected spin response [2,12] in the polyphase continuous excitation experiments, cross-loop resonators (CLR) were used. The 250 MHz resonator has been described [13] and the 1 GHz resonator is analogous, but with modified dimensions, to a previously described L-band resonator [14]. For the 250 MHz CLR containing the 16 mm aqueous sample the quality factor for the excitation resonator was $Q_1 = 6$, and for the detection resonator $Q_2 = 13$. For the L-band experiments the excitation resonator had $Q_1 = 250$, and the detection resonator had $Q_2 = 250$. At both frequencies the isolation between the two resonators was about 60 db.

To facilitate creation of the excitation waveforms, a Matlab program was written to produce files in a format that could be read by an arbitrary waveform generator (AWG). The 8-bit signal channel of the AWG was used to create the waveform with constant frequency and varying phase, determined using the Frank sequence. The length of the excitation sequences were selected to be 5–6 T_2. The spins are excited by a time-varying voltage from the AWG. At 250 MHz a Tektronix AWG2041 with maximum clock frequency of 1024 MHz gave four points per cycle. The excitation waveform had 1024 rf phases during a time of 29 μs. The AWG trigger synchronized the waveform with the Bruker SpecJet II digitizer that was run at the 1 GS/s sampling rate. The signal was amplified by 44 dB prior to the digitizer. Data analysis used 29,000 points which encompassed one full Frank sequence. At 1 GHz a Tektronix AWG7122C operating with a clock frequency 10 times the resonance frequency, gave 10 points per cycle. The excitation waveform had 256 rf phases during a time of 15 μs. An Acqiris U1084A digitizer was used with a sampling rate of 4 GS/s. The excitation waveform was amplified by 20 dB prior to the resonator and the signal was amplified by 30 dB prior to the digitizer. At both frequencies the detected signals were processed by digital phase sensitive detection [15–19]. Direct detection at the carrier frequency followed by digital phase sensitive detection has two major advantages: (i) the noise is defined by the thermal noise and the first stage high frequency amplifier; and (ii) the quadrature signals are perfectly orthogonal, which is important for analysis of polyphase excitation data.

3. Optimization of polyphase excitation

Analysis of data obtained by polyphase excitation is based on the assumption that the spin system is linear. A linear system is characterized by its impulse response function $h(t)$, which is called the free induction decay (FID) in magnetic resonance. Excitation with an arbitrary shape $x(t)$ produces a response $y(t)$ that is equal to the convolution of $x(t)$ and $h(t)$. In the Fourier conjugate frequency domain convolution becomes multiplication:

$$Y(\omega) = H(\omega)X(\omega), \tag{3}$$

where $X(\omega)$, $Y(\omega)$, and $H(\omega)$ are Fourier transforms of $x(t)$, $y(t)$, and $h(t)$. For a perfect noise-free measurement, $H(\omega)$ can be accurately restored by Fourier deconvolution: $H(\omega) = Y(\omega)/X(\omega)$. For data containing noise it is important to select $x(t)$ to avoid small values in the denominator $X(\omega)$ that would amplify noise. The best choice would be a function $x(t)$ for which

$$X(\omega)X^*(\omega) = C^2, \tag{4}$$

where C is an arbitrary real constant. The periodic polyphase sequences that satisfy this criterion are called 'perfect'. The autocorrelation of a perfect polyphase sequence is a delta-function and the absolute value of its Fourier transform is constant, $|X(\omega)| = |C|$.

3.1. Design of polyphase excitation sequence to optimize use of power

The first implementations of the Frank sequence for NMR [5] and EPR [7] used the excitation waveform shown in Fig. 2. There

were N pulses of equal duration t_p separated by gaps of $t_s - t_p$. Pulses had equal intensity and the same carrier frequency. The average power for the sequence of pulses shown in Fig. 2 can be found from Eq. (5), which differs from the expression for peak power given in Eq. (2).

$$\langle \text{power} \rangle = \frac{DN\alpha^2}{t_p T}. \tag{5}$$

It follows from Eq. (5) that to minimize average power for a given number of pulses N and sequence duration T, t_p should be maximized.

The minimum power requirement is achieved when there are no gaps and $t_s = t_p = T/N$. The end of each pulse is the beginning of the next pulse, so there are no longer discrete pulses, and the waveform becomes polyphase continuous excitation. In this case average power is equal to peak power. In the original NMR paper [5] the gaps were needed to permit collection of data after the so-called 'dead time', the time for the resonator to dissipate energy from the excitation pulse. Since nuclear spin relaxation times are much longer than the ring-down time of the resonator, data acquisition after a dead time allows separation of the spin system response from the resonator response. Electron spin relaxation lasts for about the same time as the resonator ring-down, so data are collected in the presence of the resonator ring-down. For EPR, having gaps between pulses exacerbates the background problem, because it requires more power for a similar turning angle, thus producing a more intense resonator ring-down signal. Cross-loop resonators isolate excitation from detection by 40–60 db [13,14], which decreases the resonator background signal by the amount of the isolation.

The power for Frank sequence EPR with $t_s = t_p$ can be compared with the power required for a single $\pi/2$ pulse, based on Eqs. (1), (2), and (5). The reduction is $[\pi/(2\alpha)]^2$ or $[\pi/(2\alpha)]^2/N$ for the peak or average power, respectively.

3.2. Data analysis

In the first implementation of the Frank sequence for NMR [5], one data point was acquired shortly before each successive pulse, forming an array of data points with length N (Fig. 2). In the initial EPR implementation [7] a few points were averaged between successive pulses with the goal of improving the signal-to-noise ratio, SNR. The number of data points in the resultant array again was equal to N. Cross-correlation of the data arrays and the Frank sequence produced NMR and EPR FID with N elements. Although the outcomes were demonstrated, the mathematical basis has not been discussed. A fundamental issue is that the Frank sequence is a discrete series of numbers, whereas the excitation waveform is a continuous function in which the phase changes are encoded by the sequence. The following derivation examines the implications for data analysis.

An analytical expression for the Fourier transform of the periodic continuous excitation function $x(t)$ with $t_s = t_p$ is needed. Since the function has period T, it can be represented as a Fourier series:

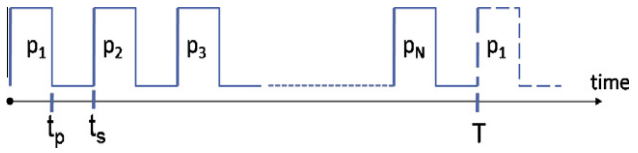

Fig. 2. Schematic of the polyphase excitation sequence. The duration of each pulse is t_p, and the entire sequence is repeated cyclically with period T. The time between the start of two successive pulses is t_s, so $t_s N = T$. Phases $p_1, \ldots, p_N$ are the elements of the Frank sequence.

$$x(t) = x(t+T) = \sum_{k=-\infty}^{\infty} X_k e^{j2\pi f_0 t}, \quad f_0 = \frac{1}{T}, \tag{6}$$

where the discrete function X_k is defined for a set of angular frequencies that are integer (k) multiples of $2\pi f_0$:

$$X_k = \frac{1}{T}\int_0^T x(t) e^{-jk2\pi f_0 t} dt. \tag{7}$$

Using the fact that the function $x(t)$ is composed of N phases (Fig. 2), Eq. (7) can be rewritten as a sum of N integrals corresponding to the N phases:

$$\begin{aligned} X_k &= \frac{e^{jp_0}}{T}\int_0^{t_s} f(t) e^{-jk2\pi f_0 t} dt + \frac{e^{jp_1}}{T}\int_{t_s}^{2t_s} f(t-t_s) e^{-jk2\pi f_0 t} dt + \cdots \\ &\quad + \frac{e^{jp_{N-1}}}{T}\int_{(N-1)t_s}^{Nt_s} f(t-(N-1)t_s) e^{-jk2\pi f_0 t} dt \\ &= \frac{1}{T}\sum_{n=0}^{N-1}\int_{nt_s}^{(n+1)t_s} e^{jp_n} f(t-nt_s) e^{-jk2\pi f_0 t} dt. \end{aligned} \tag{8}$$

Here $f(t)$ describes a square pulse with duration t_s, and p_n are the phases defined by the elements of the Frank sequence. Eq. (8) can be simplified by changing variables to $\tau = t - nt_s$, where n is the number of the pulse:

$$X_k = \frac{1}{T}\int_0^{t_s} f(\tau) e^{-jk2\pi f_0 \tau} d\tau \times \sum_{n=0}^{N-1} e^{jp_n} e^{-jn2\pi f_0 k t_s}. \tag{9}$$

Eq. (9) can be represented as multiplication of two discrete functions:

$$X_k = F_k P_k. \tag{10}$$

The first term, F_k, is the Fourier series for a square pulse with duration t_s. For a pulse with amplitude B_1, $f(\tau)$ can be set equal to B_1 in the interval 0 to t_s, and the expression for F_k can be found by integration:

$$F_k = \frac{B_1}{T}\frac{e^{-jk2\pi f_0 t_s} - 1}{-jk2\pi f_0} = \frac{t_p B_1}{T} e^{-jk2\pi f_0 t_s/2} \operatorname{sinc}(k\pi f_0 t_s), \tag{11}$$

where $\operatorname{sinc}(x) = \sin(x)/x$. The complex coefficient of the sinc function appears in Eq. (11) as a result of the asymmetry of the pulse with respect to $t = 0$. The second term in Eq. (10) is P_k,

$$P_k = \sum_{n=0}^{N-1} e^{jp_n} e^{-j2\pi nk/N}, \tag{12}$$

which is the discrete Fourier transform of the Frank sequence. It is periodic in the frequency domain with period equal to $2\pi f_0 N$ (Eq. (9)). Examination of Eqs. (11) and (12) shows that function X_k is the product of periodic function P_k and function F_k, which is not periodic, where both of these are discrete. Substitution of Eq. (10) into Eq. (3) gives:

$$Y_k = F_k P_k H_k, \tag{13}$$

where Y_k and H_k are discrete functions that are defined for the same angular frequencies as P_k and F_k.

Eq. (13) provides a basis for comparison of single pulse FID and multiphase Frank sequence experiments. For a single pulse experiment the summation in Eq. (8) is reduced to only the first term, which has $p_0 = 0$, giving

$$X_k \text{ (single pulse)} = \frac{1}{T}\int_0^{t_s} f(t) e^{-jk2\pi f_0 t} dt = F_k, \tag{14}$$

and Y_k (single pulse) becomes

$$Y_k \text{ (single pulse)} = F_k H_k \text{ (single pulse)}. \tag{15}$$

As shown in Eq. (11), F_k is proportional to B_1. Since $|P_k| = \sqrt{N}$, comparison of Eqs. (13) and (15) indicates that if the same B_1 (peak power)

is used, the signal obtained by polyphase continuous excitation in the linear response regime is $\sqrt{N}$ times larger than that obtained with a single pulse. The excitation bandwidth is the same for the two experiments.

Eq. (13) also is the basis for the cross-correlation method that was used in analyzing prior data (Fig. 1) [5,7]. In the frequency domain cross-correlation is performed by multiplication of Y_k by P_k^*, so Eq. (13) becomes Eq. (16) because $P_kP_k^* = N$. The result

$$H_kF_k = \frac{Y_kP_k^*}{N}, \tag{16}$$

is proportional to the product of EPR spectrum H_k and the Fourier transform of the excitation pulse profile (F_k). This spectrum is the same as the Fourier transform of the FID that would have been obtained with a single pulse of duration t_s. A pulse provides an excitation bandwidth of about $1.2/t_s$ (full width at half height) [20]. If the spectral width is small with respect to that bandwidth, F_k is flat in the region of interest, and cross-correlation produces an undistorted spectrum. Otherwise, the excitation profile of the pulse has to be taken into account to accurately restore the lineshape.

An alternate way to analyze the data (Fig. 1) is deconvolution where $H_k = Y_k/X_k$ (Eq. (3) but now written for discrete functions), and $X_k = F_kP_k$ (Eq. (10)) is the Fourier transform of the excitation waveform (Eq. (7)). The resulting spectrum, H_k, is unaffected by the shape of the pulse (Eq. (17)). Thus, if the excitation profile is not uniform over the spectrum, the relative amplitudes and phases of lines in the spectrum will be more accurate if data are analyzed using Eq. (17) instead of Eq. (16).

$$H_k = Y_k/(P_kF_k). \tag{17}$$

3.3. Resonator Q, background signal, and spectral window

3.3.1. Resonator Q

In a pulse experiment the resonator acts as a band pass filter. When a cross-loop resonator is used both the filtering of the excitation by resonator 1 (Q_1) and the filtering of the detected signal by resonator 2 (Q_2) must be considered. If Q for both resonators is sufficiently low, the impact on the spectrum is negligible. However, lowering Q decreases signal amplitude which decreases SNR, and decreases the resonator efficiency, which requires higher power to achieve the same turning angle (Eq. (2)). Thus the selection of Q is a compromise between these factors.

3.3.2. Background signal

The dominant contribution to the background signal is direct 'leakage' from the excitation resonator to the detection resonator, which has the shape λF_kP_k, and is the same as Eq. (13) except for the spin response. Here λ is the voltage attenuation coefficient describing isolation between the excitation and detection resonators. Depending on the CLR design, λ varies from 100 to 1000 [13,14]. The majority of this contribution is removed by subtraction of an off-resonance signal (Fig. 1), although this decreases SNR by $\sqrt{2}$. For a weak EPR signal there often is a residual background contribution to H_k, which is difficult to separate from signal in the frequency domain. In these cases H_k was inverse Fourier transformed to $h(t)$. In the time domain the decay of the background signal depends on Q_1 and Q_2, analogous to the ring-down after a single pulse. If resonator Q is sufficiently low, the background signal decays faster than the spin response so it is greater for the first few points of $h(t)$. Elimination of these points, which is similar to delaying data collection until after the 'dead time' in a one-pulse FID experiment, decreases SNR but improves lineshape. After elimination of the first few points, $h(t)$ was Fourier transformed to recover H_k with improved lineshape (Fig. 1).

If isolation is not perfect, a weak EPR signal is superimposed on a large background signal. This large signal may saturate the first stage amplifier unless it has a very large dynamic range. If the background saturates the amplifier it cannot be accurately subtracted. In addition, when the background signal is very large, the superimposed EPR signal may be less than one bit of the digitizer. The effective number of bits in the digitizer can be increased by signal averaging, but excessive averaging usually results in leakage of coherent clock signals into the digitized data. The constraints imposed by amplifier saturation and limited bits of the digitizer make minimization of the background by maximizing the isolation between resonators very important.

3.3.3. Spectral window

In previous implementations of the Frank sequence for NMR [5] and EPR [7], signal sampled with the rate $f_s = 1/t_s$ was used for cross-correlation. This limits the spectral window of H_k to the interval $[-f_N, f_N]$, where $f_N = f_s/2$ is the Nyquist frequency. This sampling could increase noise in the spectrum because of the aliasing of frequencies higher than f_N. Function X_k in Eqs. (7) and (13) is defined from $-\infty$ to $+\infty$, so the sampling frequency can be selected, independent of t_s, to define a desired signal bandwidth and avoid aliasing. There is still a limitation on the frequencies for which the EPR spectrum can be restored, which comes from the multiplication by the sinc function in Eq. (11) that has zeros at frequencies $f = mf_s$, where $m > 0$ is an arbitrary integer.

3.4. Linearity of the spin system

For a single pulse, the on-resonance magnetic field B_1 turns magnetization by an angle defined in Eq. (1). The signal measured in an experiment is proportional to the nonlinear function $\sin(\alpha)$. Increasing B_1 by a factor of two, increases the signal amplitude by a factor of $\sin(2\alpha)/\sin(\alpha)$, which is not a factor of 2. This shows that the spin system is non-linear. However, for very small turning angles $\sin(\alpha) \approx \alpha$, and the spin system approximates linear behavior. In this case Eq. (3) can be used to recover the EPR spectrum obtained by polyphase excitation with either Eqs. (16) or (17). For practical application of polyphase excitation (Fig. 1) it is important to estimate the threshold turning angle for which the deviation from linearity is so large that the use of Eq. (3) results in significant distortion of the lineshape. This limit was determined by numerical simulation with parameters based on the relaxation times for LiPc which was used in the experiments, $T_2 = T_1 = 2.32$ μs. LiPc has a Lorentzian lineshape [21]. The sequence duration T was set to $\sim 6T_2$ ($T = 15$ μs). Six T_2 instead of the $5T_2$ originally suggested [5], was used to ensure decay to baseline, provide leeway if there is a distribution of T_2 values, and provide opportunity for zero-filling, which increases spectral resolution (Eq. (6)). If there is a distribution of T_2 values, T should be selected to be at least five times the longest T_2. $N = 256$ was selected to ensure adequate signal bandwidth. Simulations were performed with the same T and N as the experiments. In the simulations it was assumed that resonator Q was low enough that its impact on lineshape was negligible.

In the simulations the Bloch equations were solved numerically for an EPR line on resonance at a series of B_1 amplitudes. Calculated M_x and M_y components of the magnetization for a full cycle were combined to form a complex function $y(t)$ that was Fourier transformed and deconvolved using Eq. (17) to obtain the EPR spectrum. In the linear response regime $h(t)$ decays exponentially to approximately baseline within the time $5T_2$. However, in the nonlinear regime artifacts extend beyond $5T_2$. To minimize the impacts of the artifacts, an apodization filter with cutoff at $5T_2$ was applied to both the simulated and experimental $h(t)$. Multiplication by that function does not noticeably broaden the signal, but reduces high frequency oscillations. Calculated H_k were fit with the Matlab

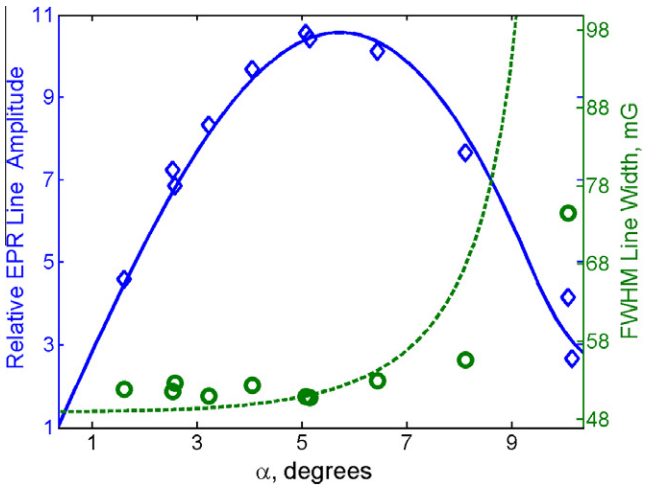

Fig. 3. Relative amplitudes (blue) and linewidths (green) as a function of turning angle α calculated for $T = 15$ μs, $N = 256$, and $T_2 = T_1 = 2.32$ μs. Simulated amplitudes (solid line) were normalized to 1.0 corresponding to amplitude at $\alpha = 90°/N$. Simulated linewidths are represented by a dashed line. Experimental values for LiPc are shown for relative amplitudes (blue diamonds) and FWHM linewidths (green circles).

nonlinear least-squares fitting routine *lsqnonlin* to obtain three characteristics: (i) amplitude, (ii) Lorentzian linewidth, and (iii) position. For the *x*-axis of Fig. 3, α was calculated from B_1 using Eq. (1) with $t_p = t_s$ and converted to degrees. The vertical axis for signal amplitude is scaled to that at $\alpha = 90°/N$ (Fig. 3, left-axis). As B_1 (and turning angle) increases, the signal amplitudes goes through a maximum and the linewidth increases, as is typical for power saturation [1]. The maximum signal amplitude occurs at $\alpha = 5.6°$ which is much larger than the $\alpha = 90°/N = 0.35°$, initially proposed as optimum for the Frank sequence [5]. At the maximum in the power saturation curve the line is broadened by about 5% and the signal intensity is about 10 times greater than at $\alpha = 0.35°$. These calculations show that the amplitude of the EPR signal can be increased by an order of magnitude, relative to that observed with the small turning angle initially proposed for the Frank sequence [5], if small lineshape distortion due to non-linearity of the spin system is acceptable. For α greater than the peak in the power saturation curve, the lineshapes were sufficiently distorted that fitting to a Lorentzian was not meaningful.

To test the simulations, spectra of LiPc were obtained by polyphase excitation at $\upsilon_0 = 1037.8$ MHz. The maximum B_1 in the resonator with this sample was measured at the full voltage output of the AWG, amplified to 4.3 Vpp. The on-resonance nutation frequency [22] gave $B_1 = 0.40 \pm 0.05$ G and the length of the pulse that maximized the amplitude of an FID gave $B_1 = 0.47 \pm 0.05$ G. B_1 was varied by using different combinations of 3, 6, or 10 db attenuators along with changing the AWG output voltage. Comparison with the calculated saturation curve (blue line,[1] Fig. 3) showed that maximum $B_1 = 0.46$ G gave the best match. This value was used to calculate the turning angles in Fig. 3. Experimental points for relative amplitudes are in a good agreement with the calculated curve. The experimental linewidths are 2–3 mG larger than that expected from the independently measured value of T_2, which is attributed to uncertainties in the measurements.

Fig. 4 shows experimental and simulated spectra corresponding to $\alpha = 5°$, which is near the peak of the power saturation curve. Since phasing of the original experimental data is arbitrary, the phase was adjusted to make the line symmetrical. The phase is accurately defined by the simulations, but there are lineshape distortions at larger values of α that contribute to the small difference between the simulated and experimental lineshapes at $\alpha = 5°$.

Parameter α is the angle by which spins at resonance are turned in an individual segment of length t_s in the polyphase sequence Eq. (1). The spin system is excited continuously with B_1 of constant amplitude, but varying phase. To show the time evolution of the spin system the cumulative phase angle, α_c, was examined:

$$\alpha_c = \frac{180}{\pi} \sin^{-1}\left(\frac{\sqrt{M_x^2 + M_y^2}}{M_0}\right), \tag{18}$$

where M_x, M_y are the *x*, *y* components of the magnetization vector, M_0 is the magnetization at thermal equilibrium, and α_c is in degrees. Parameter α_c is the net result of many phase changes and the relaxation processes. It reflects the overall intensity of the recorded signal and provides a basis for comparison of polyphase excitation and single pulse excitation with $\alpha_c = \alpha = 90°$. Fig. 5 shows the time evolution of α_c calculated with the Bloch equations, for a polyphase cycle after the spins have come to dynamic equilibrium in several prior cycles. Calculations were performed for $\alpha = 5°$. Note that at $t = 0$ for this cycle α_c is not zero because of the cumulative effect of the prior cycles.

For a sample with the relaxation times characteristic of LiPc, the signal amplitude obtained with $\alpha = 5°$ is 10 times larger than with $\alpha = 90°/N = 0.35°$ (Fig. 3). Calculations were performed to compare these amplitudes with the results expected for a single pulse with three different turning angles (Table 1). As discussed above, at $\alpha = 0.35°$ the single pulse gives a signal that is weaker by a factor of $1/\sqrt{N}$. At $\alpha = 5°$ the signal amplitude is less than 16 times the amplitude at $\alpha = 0.35°$ because of saturation. The amplitude obtained with a single 90° pulse is about the same as for the polyphase continuous excitation at 5°. The ratios are theoretical predictions. In practice the large background signal makes it difficult to achieve the theoretical advantages of polyphase excitation.

Table 2 highlights the decreased power requirements for polyphase continuous excitation. Relative to a power of 1.0 for a single 90° pulse the peak power required for $\alpha = 5°$ or $\alpha = 0.35°$ are only 0.003 and 1.5×10^{-5}, respectively. The reduction in the average power over the time of the sequence is smaller, because the power is on continuously.

The results shown in Figs. 4 and 5 and Tables 1 and 2 were calculated for $T_1 = T_2 = 2.32$ μs, $N = 256$, and $T = 15$ μs. The same results would be obtained for other cases with $T_1 = T_2$ provided that T and $1/B_1$ are scaled proportionally.

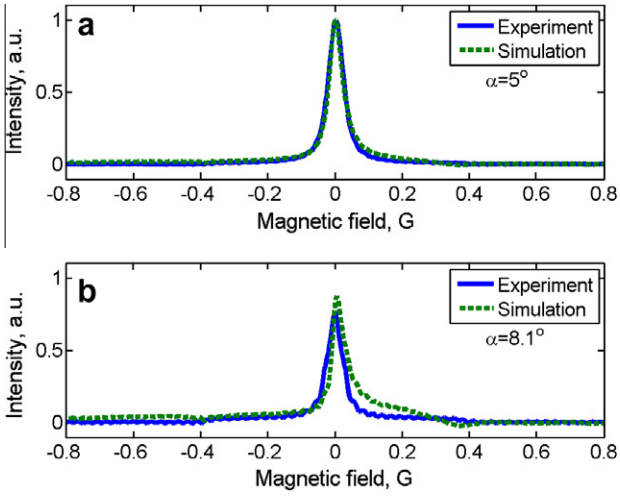

Fig. 4. Comparison of simulated (dashed green) and experimental (solid blue) LiPc spectra for turning angle $\alpha = 5°$ which is near the peak of the power saturation curve (a) and for $\alpha = 8.1°$ (b).

[1] For interpretation of color in Figs. 1–7, the reader is referred to the web version of this article.

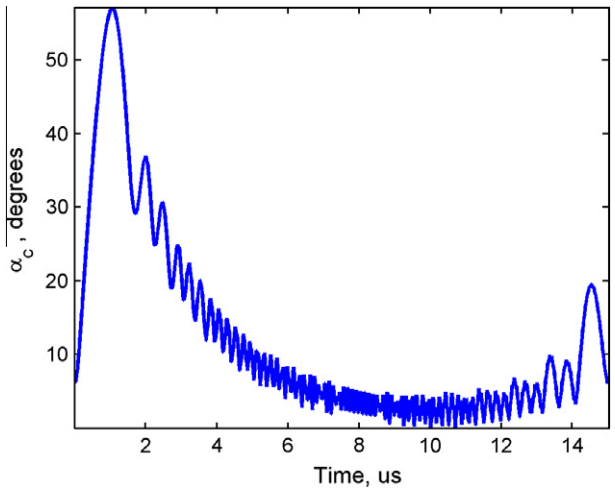

Fig. 5. Time dependence of the cumulative turning angle α_c during an excitation sequence of 256 phase changes and $T = 15$ μs, calculated using the Bloch equations for $\alpha = 5°$ and relaxation times characteristic of LiPc.

Table 1
Calculated relative EPR amplitudes compared for constant t_s.[a]

Turning angle, α	0.35°	5°	90°
Polyphase continuous	1.0	10	–
Single pulse	1/16	0.88	10

[a] Calculated for $T_1 = T_2 = 2.32$ μs, $T = 15$ μs, $N = 256$, assuming no dead time in detection. Amplitudes were scaled to that obtained with polyphase excitation at $\alpha = 0.35°$.

Table 2
Power[a] for polyphase continuous excitation relative to single pulse, constant t_s and $N = 256$.

Turning angle, α	0.35°	5°	90°[a]
Peak power	$1/(257)^2$	$1/(18)^2$	1.0
Average power	1/258	1/1.3	–

[a] Normalized to 1.0 for the peak power required for a 90° pulse.

4. Experimental results with trityl OX63

To test the generality of the method, polyphase continuous excitation was applied to deoxygenated aqueous solutions of the OX63 trityl radical at 250 MHz. The lineshapes for these spectra, which have substantial contributions from inhomogeneous broadening and resolved ^{13}C hyperfine lines, test the performance of the sequence for multi-line spectra. The experiments were performed with $N = 1024$, in the low-power linear regime.

Fig. 6 compares the spectra obtained with polyphase continuous excitation with a CW spectrum acquired with phase sensitive detection in a different resonator. The signal at 250 MHz obtained by polyphase excitation was digitized with a sampling interval of 1 ns. The resulting EPR signal was differentiated for comparison with the CW spectrum. The CW spectrum was recorded with 5 kHz modulation frequency at low modulation amplitude. The peak-to-peak linewidths of 160 mG are in good agreement for the spectra obtained by the two methods. The ^{13}C hyperfine lines with splittings of 2.44 and 1.27 G [23] are clearly observed in both spectra.

The spectrum of OX63-d_{24} measured with polyphase continuous excitation in a homogeneous magnetic field (Fig. 7a) had FWHM = 114 mG, which is in good agreement with the value observed by CW EPR. To demonstrate the possibility of polyphase

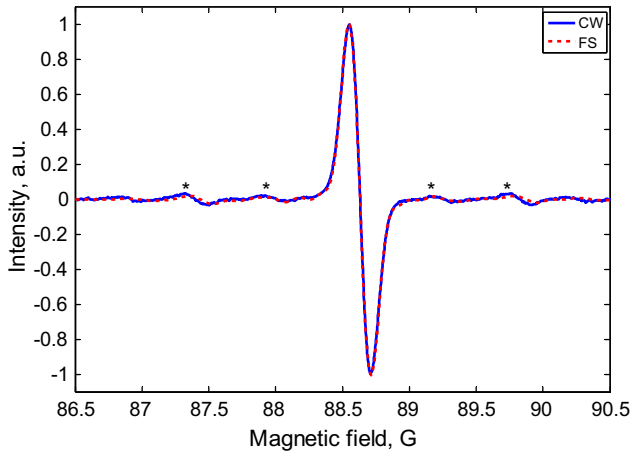

Fig. 6. Comparison of EPR spectra of OX63 at 250 MHz obtained by CW (solid blue) and by polyphase continuous excitation (red dashed) with 1024 pulses. The Q of the CLR was lowered to 6 for the excitation resonator and to 10 for the detection resonator to minimize spectral distortion and to provide large enough bandwidth to observe the ^{13}C-hyperfine lines that are marked with $*$.

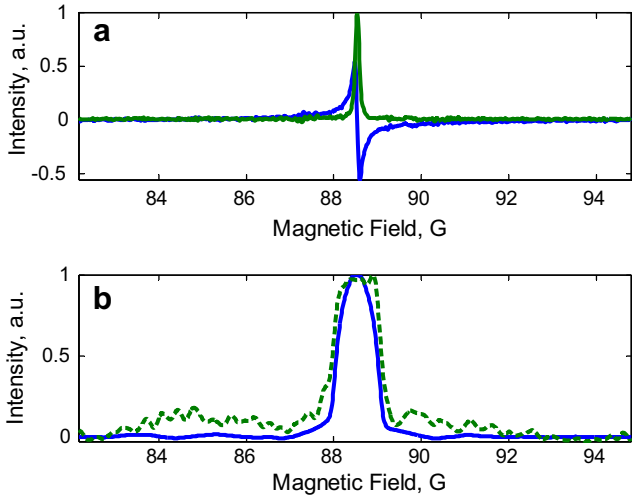

Fig. 7. EPR spectra of OX63-d_{24} at 250 MHz obtained with polyphase continuous excitation with 1024 pulses. (a) Spectrum in homogeneous magnetic field, green line corresponds to absorption and blue to dispersion signals; (b) spectrum measured in magnetic field gradient of 0.44 G/cm. The green dashed line shows the absorption spectrum, and the blue solid line is computed based on the known sample geometry and homogeneous lineshape (a) profile.

continuous excitation for EPR imaging, a 1D projection was measured in the presence of a constant magnetic field gradient of 0.44 G/cm (Fig. 7b). The experimental spectrum was compared with one that was calculated by convolution of the homogenous spectrum Fig. 7a with a 1D projection of the 25 mm tube diameter.

5. Conclusions

The energy introduced into a resonator after a single 90° pulse is many orders of magnitude larger than that absorbed by a spin system, so the spin system response is weak with respect to the resonator response. In a standard pulsed NMR or EPR experiment data collection starts after a dead time during which the resonator ring down decays to a level that is small enough to permit detection of the weak spin response. Substitution of the single 90° pulse by polyphase continuous excitation significantly reduces the amount of energy that is used for excitation. The background signal

becomes much smaller, but is present all of the time. Separation of the EPR and background signals based on the concept of 'dead time' is now not applicable during data collection. Instead, the dead time is taken into account by excluding the first few points in the time-domain data array after deconvolution or cross-correlation of the polyphase excitation data.

Mathematical analysis of the polyphase continuous excitation shows that EPR spectra can be restored by two different but closely related methods: by cross-correlation with the Fourier transform of the excitation phase sequence (Eq. (16) or deconvolution with the Fourier transform of the excitation waveform including the pulse profile (Eq. (17)), (Fig. 1). In the case of deconvolution the limitation of the sampling rate can be overcome. The deconvolution method might be more useful since it eliminates the effect of the pulse shape on EPR amplitudes and phases, which is important for EPR imaging.

If the pulse length for a single pulse is equal to t_s for the polyphase continuous excitation, the excitation profiles are the same for the two experiments. If B_1 is the same, the signal obtained with a single pulse is weaker than with polyphase excitation. Numerical solution of the Bloch equations followed by deconvolution and line fitting demonstrated that the EPR lineshape obtained by polyphase excitation is distorted and broadened as the excitation power increases. However, the amplitude of the spectrum increases faster than the linewidth in percentage terms. If a small (~5%) broadening is acceptable, the EPR signal amplitude can be increased by an order of magnitude relative to what would be obtained at the small turning angles initially proposed for Frank sequence excitation [5].

When available power is limited, as may occur when the resonator efficiency is low, polyphase excitation based on the Frank sequence excitation may be favorable. The major problem with continuous polyphase excitation is that, even with a cross loop resonator, the spin system response is still much weaker than the one induced in the resonator by the excitation. The large background signals are difficult to amplify and digitize within the linear region of the equipment, and complicate detection of the weak spin signals in the presence of the large background.

For spectral fidelity the resonator and excitation bandwidth should be large enough to encompass the entire spectrum. The power should be optimized to ensure that the spin system approximates a linear system. If additional power is available, B_1 can be increased and t_s decreased, producing a flatter profile over the region of interest. This would not contribute significantly to additional heating of the sample, because the bandwidth of resonator 1 limits the range of frequencies incident on the sample. Sequence duration T should be chosen such that the FID with the longest relaxation time decays to baseline. Since there is often some uncertainty in estimation of the longest T_2 in the sample, $T = 6T_2$ is recommended. The T value can be corrected after performing the first measurement. Increasing the sequence duration beyond $6T_2$ does not impact the lineshape but would decrease the excitation bandwidth as a result of increased t_s. Experimental testing of the polyphase continuous excitation method at 250 MHz and 1 GHz showed that it is applicable to samples with inhomogeneous line broadening and multi-line spectra. Measurement of a 1D projection with magnetic field gradient demonstrated that the method can potentially be used for EPR imaging. The resonator Q limits the excitation bandwidth. For the same Q the bandwidth increases proportional to frequency so for the same Q wider spectra can be excited at higher frequencies. However, implementation of continuous polyphase excitation at higher frequencies puts additional speed requirements on the AWG and the digitizer.

Acknowledgments

Funding for this work from NIH NIBIB Grant EB000557 (GRE and SSE) and NIH NIBIB P41 EB002034 (Howard J. Halpern, PI) is gratefully acknowledged. Samples of OX63 and OX63-d_{24} were provided by Howard Halpern, University of Chicago. The L-band cross loop resonator was constructed by George A. Rinard (University of Denver). The loan of the AWG from Tektronix and the digitizer card from Agilent Acqiris is gratefully acknowledged.

References

[1] B. Blümich, D. Ziessow, Saturation in Hadamard NMR spectroscopy and its description by a correlation function, J. Magn. Reson. 46 (1982) 385–405.
[2] T. Prisner, K.-P. Dinse, ESR with stochastic excitation, J. Magn. Reson. 84 (1989) 296–308.
[3] R.H. Pursley, J. Kakareka, G. Salem, N. Devasahayam, S. Subramanian, R.G. Tschudin, M.C. Krishna, T.J. Pohida, Stochastic excitation and Hadamard correlation spectroscopy with bandwidth extension in RF FT-EPR, J. Magn. Reson. 162 (2003) 35–45.
[4] R.R. Ernst, Magnetic resonance with stochastic excitation, J. Magn. Reson. 3 (1970) 10–27.
[5] B. Blümich, Q. Gong, E. Byrne, M. Greferath, NMR with excitation by Frank sequences, J. Magn. Reson. 199 (2009) 18–24.
[6] G.A. Rinard, R.W. Quine, S.S. Eaton, G.R. Eaton, W. Froncisz, Relative benefits of overcoupled resonators vs. inherently low-Q resonators for pulsed magnetic resonance, J. Magn. Reson. A 108 (1994) 71–81.
[7] M. Tseitlin, R.W. Quine, S.S. Eaton, G.R. Eaton, H.J. Halpern, J.H. Ardenkjaer-Larsen, Use of the Frank sequence in pulsed EPR, J. Magn. Reson. 209 (2011) 306–309.
[8] J.H. Ardenkjaer-Larsen, I. Laursen, I. Leunbach, G. Ehnholm, L.-G. Wistrand, J.S. Petersson, K. Golman, EPR and DNP properties of certain novel single electron contrast agents intended for oximetric imaging, J. Magn. Reson. 133 (1998) 1–12.
[9] P. Turek, J.J. Andre, A. Giraudeau, J. Simon, Preparation and study of a lithium phthalocyanine radical: optical and magnetic properties, Chem. Phys. Lett. 134 (1987) 471–476.
[10] V.O. Grinberg, A.I. Smirnov, O.Y. Grinberg, S.A. Grinberg, J.A. O'Hara, H.M. Swartz, Practical conditions and limitations for high spatial resolution of multi-site EPR oximetry, Appl. Magn. Reson. 28 (2005) 69–78.
[11] G.A. Rinard, R.W. Quine, S.S. Eaton, G.R. Eaton, Frequency dependence of EPR signal intensity, 250 MHz to 9.1 GHz, J. Magn. Reson. 156 (2002) 113–121.
[12] G.A. Rinard, R.W. Quine, B.T. Ghim, S.S. Eaton, G.R. Eaton, Easily tunable crossed-loop (bimodal) EPR resonator, J. Magn. Reson. A 122 (1996) 50–57.
[13] G.A. Rinard, R.W. Quine, G.R. Eaton, S.S. Eaton, 250 MHz crossed loop resonator for pulsed electron paramagnetic resonance, Magn. Reson. Eng. 15 (2002) 37–46.
[14] G.A. Rinard, R.W. Quine, G.R. Eaton, An L-band crossed-loop (bimodal) EPR resonator, J. Magn. Reson. 144 (2000) 85–88.
[15] M. Tseitlin, S.S. Eaton, G.R. Eaton, Reconstruction of the first derivative EPR spectrum from multiple harmonics of the field-modulated CW signal, J. Magn. Reson. 209 (2011) 277–281.
[16] R. Ahmad, S. Som, E. Kesselring, P. Kuppusamy, J.L. Zweier, L.C. Potter, Digital detection and processing of multiple quadrature harmonics for EPR spectroscopy, J. Magn. Reson. 207 (2010) 322–331.
[17] M.P. Tseitlin, O.A. Tseitlin, Using of digital demodulation of multiharmonic overmodulated EPR signals to improve EPR oximetry reliability, Appl. Magn. Reson. 36 (2009) 25–34.
[18] J.S. Hyde, T.G. Camenisch, J.J. Ratke, R.A. Strangeway, W. Froncisz, Digital detection by time-locked sampling in EPR, Biol. Magn. Reson. 24 (2005) 199–222.
[19] M. Tseitlin, V.S. Iyudin, O.A. Tseitlin, Advantages of digital phase-sensitive detection for upgrading an obsolete CW EPR spectrometer, Appl. Magn. Reson. 35 (2009) 569–580.
[20] A. Schweiger, G. Jeschke, Principles of Pulse Electron Paramagnetic Resonance, Oxford University Press, Oxford, 2001.
[21] J.W. Stoner, D. Szymanski, S.S. Eaton, R.W. Quine, G.A. Rinard, G.R. Eaton, Direct-detected rapid-scan EPR at 250 MHz, J. Magn. Reson. 170 (2004) 127–135.
[22] J. Huisjen, J.S. Hyde, A pulsed EPR spectrometer, Rev. Sci. Instrum. 45 (1974) 669–675.
[23] J.P. Joshi, J.R. Ballard, G.A. Rinard, R.W. Quine, S.S. Eaton, G.R. Eaton, Rapid-scan EPR with triangular scans and Fourier deconvolution to recover the slow-scan spectrum, J. Magn. Reson. 175 (2005) 44–51.